ELSEVIER

Contents lists available at ScienceDirect

Indoor Environments

journal homepage: www.sciencedirect.com/journal/indoor-environments



The effect of the ventilation rate on exposure to SARS-CoV-2 in a room with mixing ventilation

Timothy Foat a¹, Benjamin Higgins a, Suzie Abbs a, Thomas Maishman a¹, Liam Gray b¹, Adrian Kelsey b, Simon Coldrick b, Alexander Edwards c,d¹, Matthew J. Ivings b, Simon T. Parker a¹, Catherine J. Noakes along the simon T. Parker a¹, Catherine J. Noakes along the simon T. Parker a¹, Catherine J. Noakes along the simon T. Parker a¹, Catherine J. Noakes along the simon T. Parker a¹, Catherine J. Noakes along the simon T. Parker a¹, Catherine J. Noakes along the simon T. Parker a¹, Catherine J. Noakes along the simon T. Parker a¹, Catherine J. Noakes along the simon T. Parker a¹, Catherine J. Noakes along the simon T. Parker a¹, Catherine J. Noakes along the simon T. Parker a¹, Catherine J. Noakes along the simon T. Parker a¹, Catherine J. Noakes along the simon T. Parker a¹, Catherine J. Noakes along the simon T. Parker a¹, Catherine J. Noakes along the simon T. Parker a¹, Catherine J. Noakes along the simon T. Parker a¹, Catherine J. Noakes along the simon T. Parker a¹, Catherine J. Noakes along the simon T. Parker a¹, Catherine J. Noakes along the simon T. Parker a¹, Catherine J. Noakes along the simon T. Parker along the s

- ^a Dstl, Porton Down, Salisbury, Wiltshire SP4 0JQ, UK
- ^b Health and Safety Executive, Harpur Hill, Buxton, Derbyshire, SK17 9JN, UK
- ^c EPSRC Centre for Doctoral Training in Fluid Dynamics, University of Leeds, Woodhouse Lane, Leeds LS2 9JT, UK
- d School of Chemistry, University of Bristol, Cantock's Close, Bristol BS8 1TS, UK
- ^e Leeds Institute for Fluid Dynamics, School of Civil Engineering, University of Leeds, Woodhouse Lane, Leeds LS2 9JT, UK

ARTICLE INFO

Keywords: Computational fluid dynamics Cough Air change rate Disease transmission Aerosol COVID-19

ABSTRACT

Throughout the COVID-19 pandemic, guidance was to increase ventilation as a way to reduce the risk of transmission. While the benefits of ventilation, when it is used to supply fresh air or to remove virus laden air from a space, is indisputable, we show that in some circumstances it can also enhance the transport of virus from the infected to the uninfected. We used computational fluid dynamics to study exposure to SARS-CoV-2 from a person coughing, in a mechanically ventilated room with mixing ventilation, over short time periods. Models were run with three ventilation rates and two definitions for how the virus is distributed within different size droplets. These showed that up to 3 m from the person (the largest distance assessed in this work), the median exposure had a statistically significant increase as the ventilation rate was increased. For example, as the room air change rate was increased from $0.5 \, h^{-1}$ to $5 \, h^{-1}$, the median exposure after 5 min increased by a factor of 7 or 134 depending on the model settings specified. The models showed that the negative impact of mixing ventilation on exposure (i.e. increased ventilation rate leading to increased exposure) reduced with time, which brings the predictions in line with the general guidance. Ventilation measures are therefore most likely to have the greatest impact on reducing transmission in spaces where people spend longer periods of time.

1. Introduction

Throughout the COVID-19 pandemic, guidance has been to increase ventilation as a way to reduce the risk of transmission [1,2]. The main purpose of increased ventilation, in relation to disease control, is to increase the rate of supply of fresh air and to dilute and then flush-out the pathogen carrying aerosols. However, much of this guidance states that ventilation may not have much effect on near-field or close contact transmission [1,2].

Extensive work has been carried out to understand the effect of ventilation on transmission [3-19] and it is this research which forms the basis of the guidance mentioned above. It is generally assumed that most of the airborne transmission is due to small aerosol particles and that these mix uniformly across a room over the time-scales of interest. With this 'well-mixed' assumption, simple models such as that of Wells-Riley [3], can be applied. The Wells-Riley model states that

the probability of infection = $1 - \exp(-Iqpt/Q)$ where I is the number of source patients, q [h⁻¹] is the quanta generation rate, p [m³ h⁻¹] is the pulmonary ventilation rate for each susceptible person, t [h] is the exposure time and Q [m³ h⁻¹] is the room ventilation rate.

Dai and Zhao [11] applied this model to infection from COVID-19 indoors, and based on the work of Liu et al. [12], assumed that aerosol deposition was not important for transmission. They showed that a high ventilation rate is one way to ensure a low probability of infection. Furuya [6], who stated that the 'elimination' (i.e. deposition) of infectious particles was minimal compared with removal by ventilation, showed that doubling the ventilation rate in a train resulted in an approximately halved reproduction number (i.e. the expected number of cases directly generated by one case halved) for influenza.

The Wells-Riley model, still using a well-mixed assumption, has been extended to include particle deposition and other loss terms (a

E-mail address: tgfoat@dstl.gov.uk (T. Foat).

^{*} Corresponding author.

review of the Wells-Riley model is given in [9]). This extended model has been used by Rocha-Melogno et al. [14] and Jimenez and Peng [13] in their 'Aerosol-Mediated Infectious Disease Risk Assessments' and 'COVID-19 Aerosol Transmission Estimator tools'.

It is known that increased airflow in a room can lead to increased deposition of particles. Thatcher et al. [5] showed increased deposition for particles up to $10\,\mu m$ in diameter (the largest particles assessed in their experiment) in a furnished and unfurnished room as the airflow in the room increased. Lai and Nazaroff [4] showed that turbulence close to a smooth surface increased deposition, with an upper size limit for this effect of around $0.3\,\mu m$ for deposition on upward-facing horizontal surfaces. Blocken et al. [15] calculated an increase in particle deposition with an increase in the ventilation rate, from experimental data recorded in a gym. Blocken et al. did not provide an upper limit for the effect and only presented data for particles up to $10\,\mu m$ diameter.

The size dependence of these effects is important, as it was shown previously [20] that reasonably large droplets can travel significant distances. For example, droplets with an initial diameter of $63\,\mu m$ often travelled more than 3 m from a coughing person before depositing on the floor, when the relative humidity in the room was low (30 % or 50 %). Depending on how the virus is distributed within the different size exhaled droplets, these droplets could present a significant hazard and may be expected to exhibit very different behaviours to much smaller droplets.

Turbulence can act to either increase or reduce a particle's settling velocity as it interacts with vortices in the flow. The settling velocity is the velocity a falling body reaches when gravitational and drag forces are in balance. A higher settling velocity for particles near an upward-facing horizontal surface will result in increased deposition. Good et al. [21] showed that these effects can occur (in isotropic turbulence) for a particle density to fluid density ratio of 1000, i.e., water droplets in air. Whether it increases or reduces the settling velocity is dependent on the particle diameter and the amount of turbulence.

Some modelling studies have shown that increased airflow can counter the sedimentation (the downward movement of particles under gravity) of larger particles. Chao et al. [7] carried out computational fluid dynamics (CFD) modelling of coughed droplet transport in a hospital ward and found that the higher air change rate (ACR) (11.6 h $^{-1}$ vs $6.0\,h^{-1}$) resulted in less sedimentation of droplets in the $28\,\mu m$ to $45\,\mu m$ size range due to increased vertical mixing. They also concluded that the rate of lateral spread was slower for the lower ACR, for $1.5\,\mu m$ to $45\,\mu m$ diameter droplets.

Other studies have suggested that increased ventilation could have the opposite effect of that desired. For example, Jimenez and Peng [13] wrote that increased ventilation (or mixing) can have the effect of spreading the virus faster, but they also noted that there would be a compensating effect of increased deposition. Sze To et al. [8] showed from aerosol experiments in a mock-up aircraft cabin that increased ventilation generally resulted in reduced local exposure (over a six minute period), but increased exposure for passengers seated further away. Pantelic and Tham [10] carried out experiments in a full-scale room and reported that increasing the ventilation rate from $6\,h^{-1}$ to $12\,h^{-1}$ increased aerosol exposure at all distances from the source examined (1 m to 4 m). Wei et al. [16] conducted a CFD study of exposure to respiratory droplets in a mechanically ventilated room and showed that increased ventilation reduced the small droplet (5 μm diameter) exposure, but increased the exposure to medium droplets (30 µm to 50 µm diameter depending on the proximity to the infected person and the ventilation rate). The causes of the effects in [8,10,16] were given as: increased ventilation resulting in increased dispersion, increased droplet evaporation or changes in the airflow pattern in the space. Li et al. [17] carried out experiments to assess the effect of ceiling fans on the transmission of infectious aerosol. They showed that the addition of the fans reduced the short-range infection risk by 47 %, but increased the long-range risk by 4 %. Conversely, a CFD study by Omerzo et al. [18] showed in a mixing or displacement ventilated

room that the airborne transmission risk reduced by $50\,\%$ when the air change rate was increased from $0.5\,h^{-1}$ to $1\,h^{-1}$. There was a further $27\,\%$ reduction when the air change rate was increased to $2\,h^{-1}$ and a further $15\,\%$ reduction at $4\,h^{-1}$. In the Omerzo et al. [18] study they only considered a steady-state case with continuous exhalation of a tracer gas representing the infectious aerosol. Yao et al. [19] carried out a CFD modelling study to compare different ventilation strategies in a dental clinic. They showed that with some ventilation modes the aerosol removal index (a measure of how effectively aerosol is removed from the space) reduced as the room ventilation rate was increased from $6\,h^{-1}$ to $12\,h^{-1}$.

All the CFD and room scale experimental studies described above have correlated risk or effect with the droplet or particle concentration. This approach is valid if the concentration of infectious material in the droplets is proportional to the droplet's volume. However, a number of studies have suggested that people infected with both influenza and SARS-CoV-2 may produce more virus in the fine aerosol fraction (diameters $\leq 5 \, \mu$ m) than in the coarse fraction (diameters $>5 \, \mu$ m) [22,23]. If proportionally more virus is carried in the smaller droplets, this could have a significant effect on the hazard, as smaller droplets are likely to be dispersed more effectively and to remain airborne for longer [20].

To address this research gap, we have used CFD methods developed previously [20,24] to model a coughing person in a mechanically ventilated room to show the effect that the ventilation rate has on exposure to SARS-CoV-2. The CFD results are reported in terms of viral exposure rather than droplet number or mass and two definitions for how the virus is distributed within different size droplets have been applied. The model provides spatial resolution, predicts the rate at which droplets are transported across the room and the rate at which they evaporate and deposit onto surfaces. Consequently, it can provide details of the near-field effects which simpler models, e.g. well-mixed models, cannot. This work provides new insights into the complex interactions between ventilation and exposure that is not available elsewhere.

2. CFD methodology

2.1. Model and geometry

The effect of air change rate on exposure to the SARS-CoV-2 virus was studied in a simplified mechanically ventilated meeting room/of-fice space, based on the room studied in [20]. The room was 13.0 m long, 7.0 m wide and 2.6 m high with a small cut-out in one corner. The room volume was approximately $237\,\mathrm{m}^3$ and had mixing ventilation. The air was supplied through eight diffusers and extracted through four, which were all located on the ceiling. All supplies and extracts were square, four-way diffusers. In order to allow more generic conclusions on the hazard to be drawn, the space contained no furniture.

A coughing person was standing in the room at x = 3.5 m, y = 10 m and was facing along the long axis of the room in the negative y-direction (see Fig. 1). Three ACRs were chosen, $5\,h^{-1}$, as this was used in a previous study [20], $0.5\,h^{-1}$ as a rate which is typical of a residential space [25] (recognising that a residential space might not be mechanically ventilated) and $2.5\,h^{-1}$, as an intermediate point between the two.

The CFD modelling was carried out as described in [20]. An unsteady Reynolds averaged Navier–Stokes (URANS) approach was used to model the airflow. The transport of the exhaled virus carrying droplets was calculated using Lagrangian particle tracking, including a discrete random walk model to represent the effect of the turbulence. The simulations included buoyancy effects, driven by the heat of the person and the temperature of their exhaled breath. Buoyancy effects were modelled using an incompressible ideal gas model, where the local density is a function of temperature. The shear-stress transport (SST) turbulence model was used and the modelling was carried out using ANSYS® Fluent® version 2019 R2.

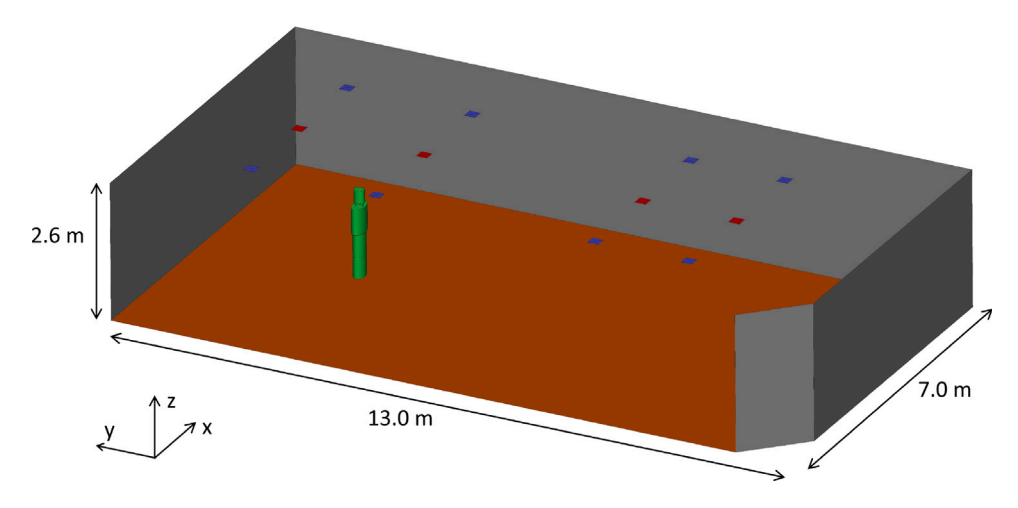


Fig. 1. The coughing person standing in the meeting room. The supply vents are shown in blue and the extracts in red.

Although a URANS model does not capture the finest detail of the airflow and mixing, it was chosen because it can provide resolution at an informative and practical computational scale. It was not feasible to use a higher resolution approach, such as large-eddy simulation, due to the size of the domain and the total simulation time. In the SST model, a $k-\omega$ model is applied near walls and a $k-\varepsilon$ model elsewhere. With the SST model, Fluent[®] automatically applies a blended wall function for the velocity and ω , switching between a viscous sublayer formulation and a wall function, depending on the near-wall cell size. The SST turbulence model was chosen based on earlier simulations [26,27] of experimental test cases for buoyancy-driven flow in a room [28] and an isolated turbulent jet [29].

The coughing person was represented by a simplified geometry and they were 1.63 m tall, with their mouth centred at 1.43 m high. The mouth was represented by a circle with a diameter of 2.25 cm. The person was located at the middle of the room width-wise, but there was an asymmetry in the room due to the cut-out in the corner and the fact that the supply and extract vents were slightly off-centre.

The susceptible people were not explicitly represented in the model and as a result it will not capture any effects they have on the flow and particle dispersion. It is recognised that thermal plumes from the susceptible people and the mixing generated by their movement could have an impact on the room airflow. However, fixing their locations would create an airflow pattern that is correct for only that specific layout. This would mean that it would not be possible to draw more generic conclusions that could be applied to any layout. Also, including the susceptible people would mean that exposures could only reasonably be calculated in the breathing zone next to each person. By excluding them, the exposure can be calculated at any location, which allows its spatial variation to be studied more effectively.

As described in [20], the geometry was meshed using unstructured tetrahedral cells in a region around the person, with hex-core in the rest of the room. It is important that care is taken to refine the mesh in areas where velocity or temperature gradients are large, and to this end, the mesh was refined around: the exhaled jet, the supply and extract vents, the person and the walls, floor and ceiling. The surface mesh on the mouth had triangular cells with lengths of approximately 2 mm, giving ten cells across the diameter of the opening. The surface mesh on the rest of the person had an average length of 12 mm. Four inflation layers were applied to all surfaces, and around the person the first cell height was on average 4.6 mm. The average y^+ (the non-dimensional near-wall cell distance) on the body surface was between 4.3 and 4.5 (i.e. within the viscous sub-layer) depending on the air change rate. The largest cell in the domain had a length of 0.126 m and the total cell count (for the standard mesh) was 3.2 million. Images of the computational mesh are shown in Fig. 2.

Models were run with three different meshes and an ACR of $5\,h^{-1}$ to check for mesh sensitivity. The mesh was coarsened by increasing all cell sizes, including inflation layers, by a factor of 1.25 and was refined by reducing all sizes by a factor of 0.5. This resulted in models with 2.3 million cells (coarse mesh), 3.2 million cell (standard mesh) and 12.6 million cells (refined mesh). The time averaged velocity was calculated on a horizontal line passing through the middle of the mouth of the person and this data is shown in Fig. 3. For the mesh dependency study, the person was not coughing.

The figure shows that the velocity did change as the mesh was refined, but the overall patterns in the flow were consistent. The peak velocity, representing mainly the thermal plume moving by the person, only varied between $0.24\,\mathrm{m\,s^{-1}}$ and $0.25\,\mathrm{m\,s^{-1}}$ and was always located 0.02 m in the front of the person. The velocity dropped rapidly within 0.2 m or 0.3 m of the person and the average across the rest of the room was consistently low; it only varied between $0.026\,\mathrm{m\,s^{-1}}$ and $0.35\,\mathrm{m\,s^{-1}}$. Therefore, as the three meshes predicted similar flow patterns, the standard mesh was the one that was taken forward.

Additional mesh dependency analysis for the same model was reported in [20] using predicted viral exposures. In that work it was reported that due to the unsteadiness in the airflow in the room and the resulting variability in the particle tracks following each cough, there was a natural variability in the results between simulations, even with the same mesh. In the current work, this variability was reduced by averaging data over more coughs, as described in the following section.

2.2. Boundary and initial conditions

The room supply vents were defined as mass-flow inlets with air entering the room at 30° to the horizontal in four directions, with $5\,\%$ turbulent intensity and a length scale of 0.01 m. The entry angle was based on the ceiling diffusers in the experimental test room described in Section 2.3. The supplied air was $20\,^{\circ}$ C and had $50\,\%$ relative humidity. The extract vents were defined as pressure outlets. Srebric and Chen [30] showed that good quality airflow predictions from a square ceiling diffuser in a room could be achieved if the momentum of the jets exiting the diffuser are correctly represented. The use of this approach is supported by the validation described in Section 2.3. Other methods for modelling square diffusers are presented in Yao et al. [19].

It was assumed that the infected person was fully clothed, and that their radiative heat transfer was negligible. Therefore, only their convective heat flux was modelled and this was applied as a uniform surface heat flux of $25\,\mathrm{W\,m^{-2}}$. This value is similar to that specified by Zhu et al. [31] for a standing person and was used in [24]. It is recognised that this is a simplification, as it is known that radiation can have an effect on indoor airflows, particularly in rooms with low-speed

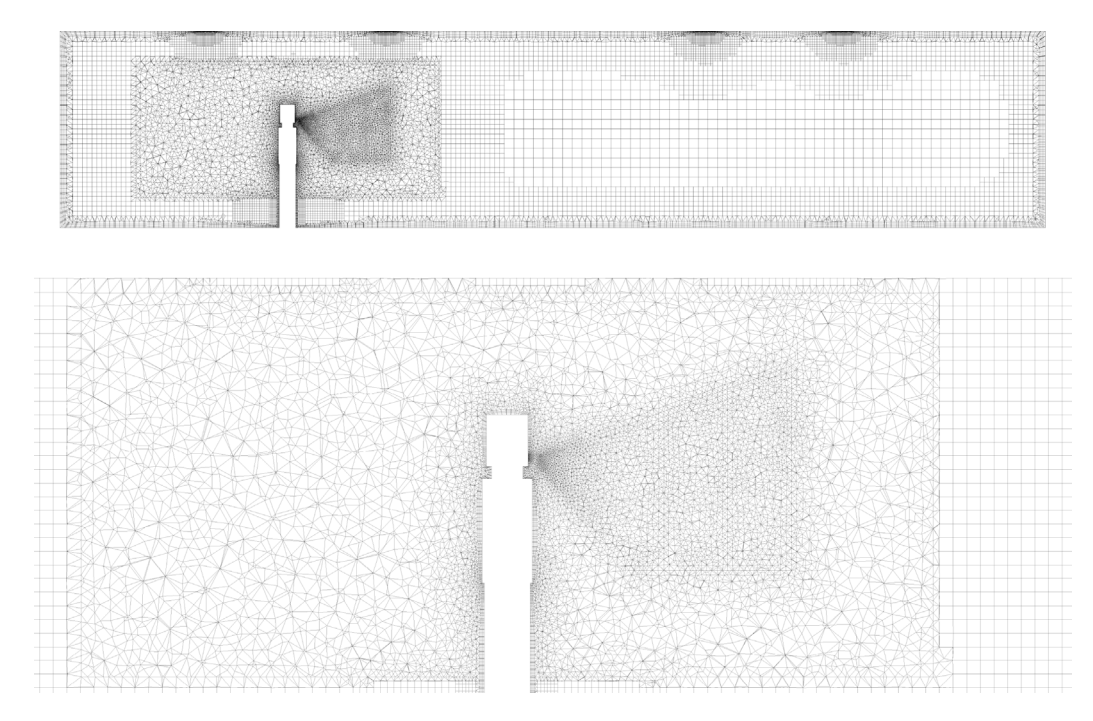


Fig. 2. Computational mesh on a vertical plane through the centre of the person. Upper image shows the full room and lower image shows details close to the person.

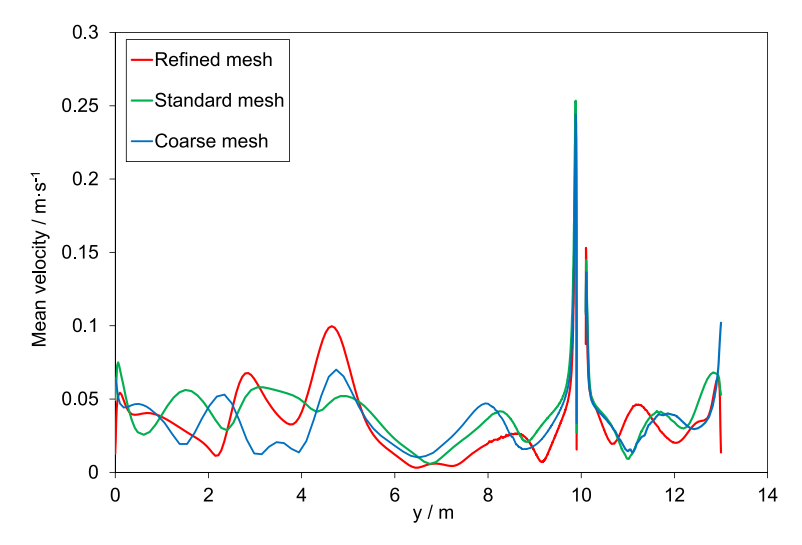


Fig. 3. Time averaged velocity on a horizontal line passing through the middle of the mouth of the person. The person is centred at y = 10 m. Data is shown for the three different meshes.

air movement. Radiation can result in increased air temperatures across the room and a resulting decrease in stratification. The walls, floor and ceiling were assigned adiabatic boundary conditions.

To represent a cough, the mouth was a velocity inlet with a time varying velocity profile (peak velocity of $15\,\mathrm{m\,s^{-1}}$, see [20] for more details) and the exhaled droplet source term was based on the bronchiolar, laryngeal and oral (BLO) model [32]. The exhaled droplets were modelled as water droplets with a non-volatile fraction, so their evaporation rate was based on the vapour pressure of pure water, and their size reduced until only the solid non-volatile core remained. The non-volatile core represents the salts, proteins and surfactants in the droplets. This fraction was set to $1.25\,\%$ by mass [33] and in light of the limited data available, it was assumed that the density of the non-volatile core was $1000\,\mathrm{kg}\,\mathrm{m}^{-3}$.

The BLO-fitted size distribution consisted of 21 logarithmically spaced initial diameters, d_0 , from 0.25 μm to 398 μm . However, due to

the shape of the BLO distribution, two of the size bins (10 μm and 14.5 μm diameter) contained no droplets.

In Lagrangian particle tracking, each computational particle can represent a parcel of droplets. This is usually done to reduce the total number of particles that need to be simulated. However, for the BLO coughing model, only 310 droplets were exhaled per cough. As this was not likely to provide a statistically significant number of droplets, ten times as many droplets were tracked per cough (3093 in total), with each droplet carrying one tenth the viral RNA copies.

Each simulation consisted of ten coughs, with each cough followed by either 5 min or 30 min of mixing. The particles from each cough were deleted at the end of the mixing period. This was done to enable the average effect of a single cough to be calculated. Spacing out the individual coughs in time, as opposed to modelling all ten coughs simultaneously, meant that the airflow in the room was different for every exhalation. The modelling in [20] showed that the exposure

predictions had not fully converged after five coughs, so the number of coughs was increased to ten for this work. It is recognised that an infectious person may cough more frequently than once every 5 min or 30 min, but the aim of this modelling was to simply study the average exposure from a single cough.

It was assumed that particles would stick to any solid surface they contacted and that there was no resuspension of deposited particles. Particles were removed from the domain if they contacted a surface. It is recognised that isotropic turbulence models, such as the SST model, can over-predict the turbulent deposition of small particles [34]. However, in these simulations the main depositional losses were due to sedimentation of the large and intermediate size particles onto the floor.

The cough jet was angled below the horizontal [35], which is only one of many possible orientations. Only the exhalation part of the cough was modelled. During the mixing period after each cough, there was no air movement from the mouth. It is reasonable to ignore the hazard from the droplets exhaled from breathing during the mixing period because the total volume of exhaled droplets over 5 min of breathing is significantly smaller than that from a single cough. The detailed properties of the cough, exhaled droplets and simplifying assumption are given in [20].

The results are expected to depend on the droplet size distribution that was used to represent what is exhaled during a cough. It would be interesting to repeat the work with different size distributions, such as described by Duguid [36], which has a higher proportion of droplets in the mid-size range.

The flow in the room was first solved as steady-state, then the model was run using an unsteady solver for 290 s with $\Delta t = 1$ s, followed by 10 s with $\Delta t = 0.1$. Then to capture the dynamics of the cough and the initial droplet transport, the model was run for 10 s with $\Delta t = 0.01$ s. The time step size was finally increased to 1 s for the duration of the mixing period. Apart from the steady-state phase, this process was repeated for each cough.

When Δt was 1 s, the average Courant–Friedrichs–Lewy (CFL) numbers in the domain for the ACR = $5\,h^{-1}$, $2.5\,h^{-1}$ and $0.5\,h^{-1}$ models were 1.7, 0.81 and 0.19 respectively. During the cough, the highest CFL numbers around the mouth were approximately 300, but these were only in the smallest cells very close to the mouth and were only present while the velocity of the cough was at its maximum.

The results of a time step size dependency study are given in [20]. For this analysis, the ACR = $5 \, h^{-1}$ model was run with three different time step conditions. The standard time step sizes were as reported above. For the shorter time step condition, all Δt values were divided by two and for the longer time step condition, all Δt values were doubled.

It was shown that there was some dependence of the predicted viral exposures to Δt , but there were no consistent trends in the data as Δt was refined. The Foat et al. [20] analysis was carried out using data from only five coughs as opposed to the ten coughs used in the current work. It is expected that the results would be more consistent across the three time step conditions if ten coughs were used. As a results of the analysis in Foat et al. [20], the standard time step sizes were taken forward in this study.

2.3. Validation

The work presented here builds on the CFD modelling of Coldrick et al. [24] and Foat et al. [20]. In Coldrick et al. [24] the CFD methodology was validated using measured surface deposition and airborne concentrations of exhaled bacteria carrying droplets from speaking, singing and coughing human subjects in an exposure chamber. As reported in [24], the conclusions of the validation were as follows. Comparisons with a human participant study showed that the model is able to produce realistic predictions of microbial surface deposition and concentrations in air, although it may slightly under-predict the

distance travelled by both aerosols and droplets. Given the uncertainties involved in simulating these experiments, the computational results obtained on the centreline were particularly encouraging. The discrepancies seen off-axis require further investigation to understand the variability in the experimental study deposition results.

In Foat et al. [20] the CFD method was validated using tracer gas dispersion data from an experiment which took place in the meeting room being studied here. In the experiment, a tracer gas was released in the corner of the room for 180 s and its concentration was monitored around the room using photo-ionisation detectors (PIDs). The CFD model was run with steady-state airflow and isothermal conditions. Fig. 4 shows the minimum, mean and maximum concentrations for all the monitor locations at each time point. Further details of the experimental method are given in [20].

As reported in [20], the CFD did not capture some of the unsteadiness in the concentration field, as would be expected when using a steady RANS modelling approach, but captured the trends well. The model over-predicted the highest concentrations (close to the gas release point). The model also predicted too much mixing, as can be seen from 400 s. However, the relative separation of the experimental curves after this point, compared the separation of the model data, may be due to instrument calibration, rather than be a true effect of the gas dispersion. The model performance was assessed by calculating the geometric mean bias and geometric variance [37] for all monitor locations and time points when the measured concentration was greater than 1 mg m^{-3} . This was approximately the lowest concentration at which the PIDs were calibrated. The mean bias was 1.12 (compared to an ideal value of 1), which indicates that the model tended to slightly under-predict the experimental data. The geometric variance was 1.10 (compared to an ideal value of 1), which indicates that there was a small amount of scatter of the model data around the experimental data.

The purpose of the current modelling study was to predict the general effect of air change rate on the dispersion of exhaled droplets in a mechanically ventilated meeting room with mixing ventilation. The validation work, together with the model sensitivity assessments have demonstrated that the modelling method applied here is fit-for-purpose. The validation work reported here and in Coldrick et al. [24], supports the selection of the SST turbulence model.

2.4. Viral load and exposure

The viral exposure [RNA copies s m⁻³] was calculated as in [20] and used two definitions for the initial distribution of the virus within the different size droplets. The first assumed a droplet volume based viral load concentration, c_V [RNA copies m⁻³]. Without there being a consensus for why there could be more virus in the fine aerosol fraction, a droplet surface area based viral load concentration, c_{SA} [RNA copies m⁻²], was chosen as the second definition to test the sensitivity of the results to the viral distribution. It has been reported, for example, that hydrophobic particles, which would be located on the surface of a water droplet would result in the particle-in-droplet concentration scaling by surface area rather than the volume [38]. Defining the viral load in terms of a surface area concentration results in a relative increase in virus in the fine aerosol and a decrease in the coarse aerosol, but it may not produce the high ratios reported by [22,23].

For the volume based viral load calculations, c_V was set to 2.76×10^9 RNA copies mL $^{-1}$, based on data from [39] which represents an average of peak viral loads over time (see [20] for more details). For the droplet surface area viral load, c_{SA} was specified so that the total amount of viral RNA in all droplets combined was the same for both viral load definitions. This gave $c_{SA}=1.17\times10^{11}$ RNA copies m $^{-2}$. This was equivalent to 2.8×10^{12} RNA copies m $^{-1}$ for the smallest droplets and 1.77×10^9 RNA copies m $^{-1}$ for the largest droplets. For both viral load

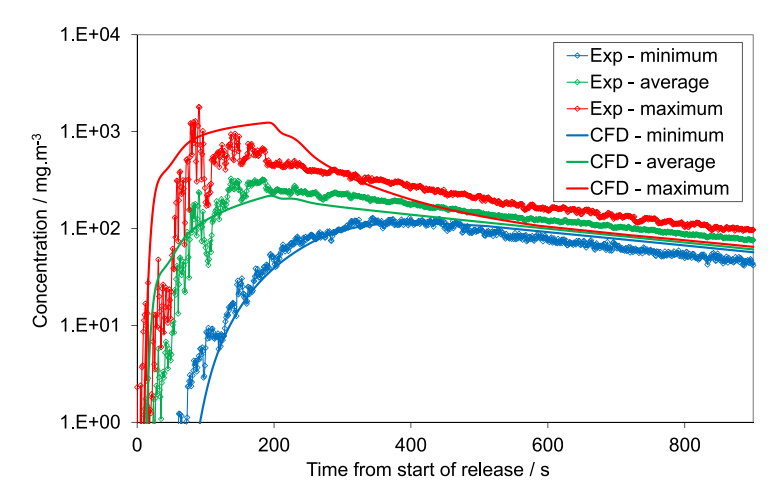


Fig. 4. Measured maximum, average and minimum tracer gas concentrations for all monitor locations compared to predictions from the CFD model. Graph from [20].

definitions, the total amount of virus exhaled in a single cough was 2.2×10^5 RNA copies.

The decay in the viability of the virus in droplets was not considered as part of this work. This is a reasonable assumption based on existing data for the viral decay half-life for SARS-CoV-2 and the duration of the simulations. For example Smither et al. [40] gave a half-life range of 30 to 177 min for SARS-CoV-2 aerosolised in artificial saliva, in the dark, with two relative humidity ranges (40% - 60% and 68% - 88%).

2.5. Summary of assumptions and simplifications

In summary, the key model simplifications were:

- Only a single coughing person was included and they only coughed once during a five minute or 30 min exposure period.
- Only one droplet size distribution has been used. This was based on the bronchiolar, laryngeal and oral (BLO) model [32].
- The person coughed with a direction below the horizontal, which is only one of many possible orientations.
- The susceptible people were not explicitly represented in the model and exposure at particular locations was used to represent risk.
- No furniture was included in the room.
- The geometry of the supply diffusers was not explicitly represented in the model.
- Exhaled droplets were modelled as pure water with a non-volatile core.
- There was no movement of people in the model and consequently no mixing created by this movement.
- A URANS approach, along with an isotropic turbulence model, was used to model the airflow.

3. Results and discussion

In the following sections, the results from the modelling are presented and discussed. Firstly, the airflow within the room is illustrated to show how it varies for the three ventilation rates. Secondly, the tracks that small, mid-size and large particles (size ranges for these are given below) follow are plotted to demonstrate their very different behaviour (irrespective of how much virus they contain). Thirdly, we provide graphs showing how the total amount of virus within the room changes with time. This shows the whole-room effect of changing the ventilation rate, without any consideration for the spatial variation. Fourthly, particle data is combined with information on the viral load to show what exposure someone in the room could receive and how this varies spatially and temporally. Finally, exposure data within three 1 m³

volumes in front of the coughing person (as used in [20]) is analysed to summarise the effect that changing the ventilation rate has on exposure in the near-field.

3.1. Flow fields

Instantaneous velocity contours from models run at the three different ACRs are shown in Fig. 5 and turbulent kinetic energy contours are shown in Fig. 6. At the mid and high ACRs, the air travels along the ceiling before being deflected down when it meets either another supply jet or a wall. This flow pattern is what drives most of the mixing within the room. The flow patterns change with time and the largest variation is seen where jets from two supply vents meet.

At the low ACR, the ceiling attached jets do not form and the weakness of the flow means that air from the top of the room does not mix effectively with the air in the lower half of the room. This results in very low air velocities and turbulence, particularly in the lower half of the room. In all three cases, the thermal plume produced by the person can be seen, but it is weakest in the high ACR case.

It should be noted that the three cases do not simply present a linear scaling of the magnitude of the air velocities in the room; the airflows are qualitatively different. A similar non-linear effect was shown in the CFD models of Wei et al. [16].

3.2. Particle tracks

The tracks for the exhaled droplets are shown in Fig. 7 for one of the ten coughs. It should be noted that there is a high amount of variability in the particle tracks for each cough (due to transient variability in the ventilation flow) and this is why the results from ten coughs were combined for the exposure analysis. The tracks have been split into three broad size bins based on their initial diameter, d_0 . These are $d_0 \leq 20\,\mu\text{m}$, $20\,\mu\text{m} < d_0 \leq 100\,\mu\text{m}$ and $d_0 > 100\,\mu\text{m}$. These were chosen to represent the small aerosol, the intermediate sizes and the large ballistic droplets. It should be noted that there were far fewer particles in the two larger diameter size bins compared to the smallest bin (2902, 73 and 118 particles in each of small, intermediate and large size bins respectively).

Due to their non-volatile core (1.25% by mass), the droplets can evaporate to approximately a quarter (23%) of their initial diameter.

It is clear that the particles with $d_0 \leq 20\,\mu\mathrm{m}$ and $20\,\mu\mathrm{m} < d_0 \leq 100\,\mu\mathrm{m}$ are affected by a change in the ACR. The droplets with $d_0 > 100\,\mu\mathrm{m}$ move ballistically and are not affected to any significant amount by the change in ACR. For both the small and intermediate size droplets, an increase in ACR results in them being mixed more widely across the room. At the lowest ACR, the smallest droplets remain close to the

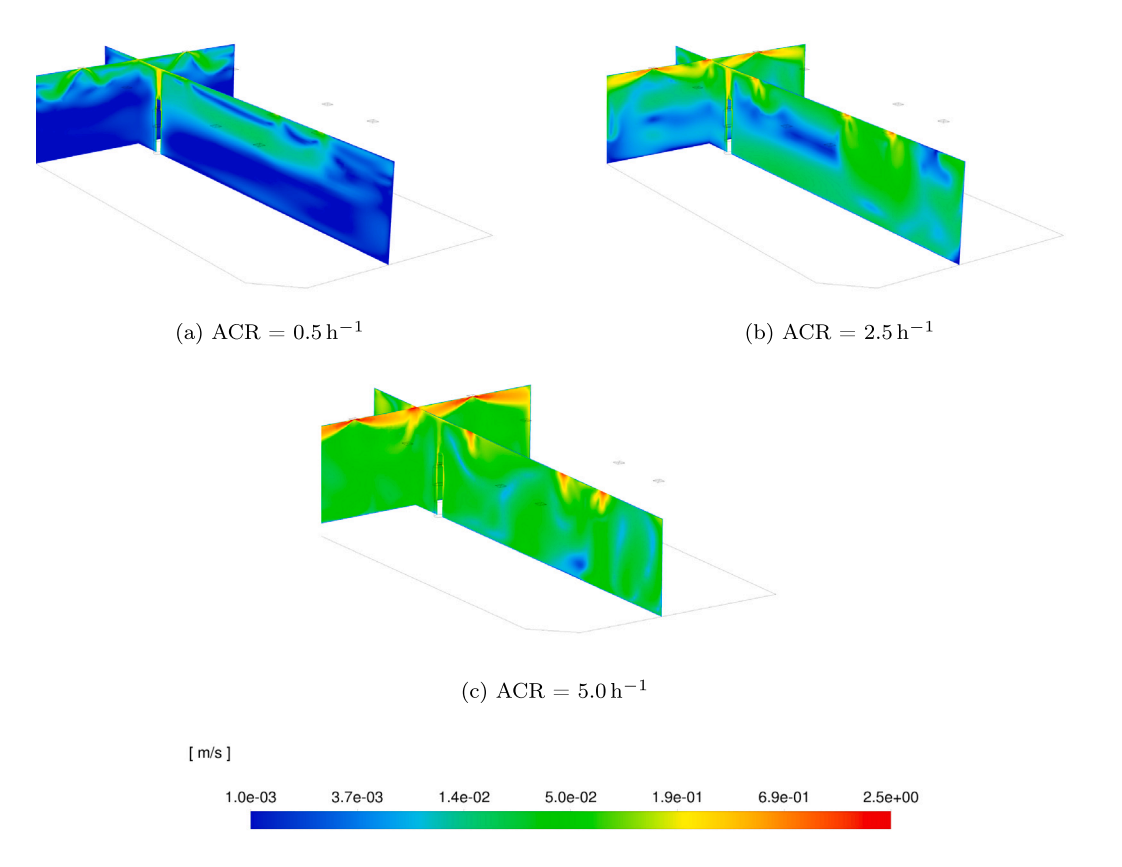


Fig. 5. Instantaneous velocity contours (on a log scale) on vertical planes through the middle of the person and one row of supply vents for all three ACRs. The upper limit was chosen to show the maximum velocity in the $5\,h^{-1}$ model and the lower limit was set to $1\,\mathrm{mm\,s^{-1}}$.

person, whereas at the highest ACR, they are dispersed widely across the room within 5 min. As would be expected, the small droplets are mixed most effectively, due to their low settling velocities and short relaxation times. An increased ventilation rate resulting in increased dispersion was also reported by Sze To et al. [8] in an experimental study in a mock-up aircraft cabin and by Chao et al. [7] in a CFD model of a hospital ward.

The behaviour of the exhaled particles close to the person are clearly shown in the plots of the intermediate sized particles. For these particles it can be seen that they are exhaled and move downwards in the direction of the cough. As the ACR is increased and the ventilation flows reach the lower part of the room, the exhaled jet becomes disrupted and penetrates a shorter distance across the space. For the low and middle ACRs, some of the intermediate size particles can be seen to be transported in the person's thermal plume towards the ceiling. At the highest ACR the particles are more effectively mixed into the room and fewer appear to sediment fully towards the floor.

3.3. Total viral RNA in the room

The total amount of viral RNA in the room was calculated to see how this evolved in time as shown in Fig. 8. The analysis shows the global effect that the ACR has on the amount of virus in the room over time, without representing any spatial information. Graphs are included with the amount of RNA calculated using either the volume and surface area viral load definitions.

Both graphs show an early rapid decrease in the amount of virus in the room as the large particles deposit onto the floor. This is followed by a second phase when the remaining particles leave the domain by either depositing on surfaces or by being extracted from the room via the ventilation system (both at a much lower rate than in the initial large particle deposition phase). Irrespective of whether the viral load is based on the droplet volume or surface area, a higher ACR initially results in a slower reduction in the amount of virus in the room. This effect is driven by the behaviour of the intermediate size particles as discussed below. The duration over which the amount of virus is higher in the high ACR case is approximately 12 min when c_{SA} is used and approximately 24 min when c_V is used.

This switch at 12 or 24 min, brings the CFD model predictions in line with the general expectation that increasing the ventilation rate is an effective way of reducing the risk of transmission. Globally, after a certain duration, there is less virus in the air when the air change rate is higher, compared with a lower ACR. However, it should be noted that by the time this point has been reached, the total amount of virus in the room has already dropped significantly, so any change that happens after this might have less effect on the exposures people receive.

The total viral count graphs are broken down into small, intermediate and large droplet size bins in Figs. 9 and 10. It is clear in these graphs, that for both viral load definitions, the rate in the second phase is governed by the intermediate size particles. This is because, even with the viral load based on the surface area, once the largest particles have deposited onto the floor, most of the remaining virus is carried in these mid-size particles. The loss rate of the smallest particles increases with the ACR. For the intermediate sizes, the effect is more complex, but at least for the first 10 min, the loss rate is slowest at the highest ACR. It should be noted that the results for the intermediate sizes at later times are less clear due to the relatively small number of particles in this size bin.

Analysis was carried out to indicate the location at which particles leave the domain or their final position at the end of a 30 min simulation for the high ACR case. This showed that all the largest particles are eventually deposited on the floor. Most of the smallest particles were

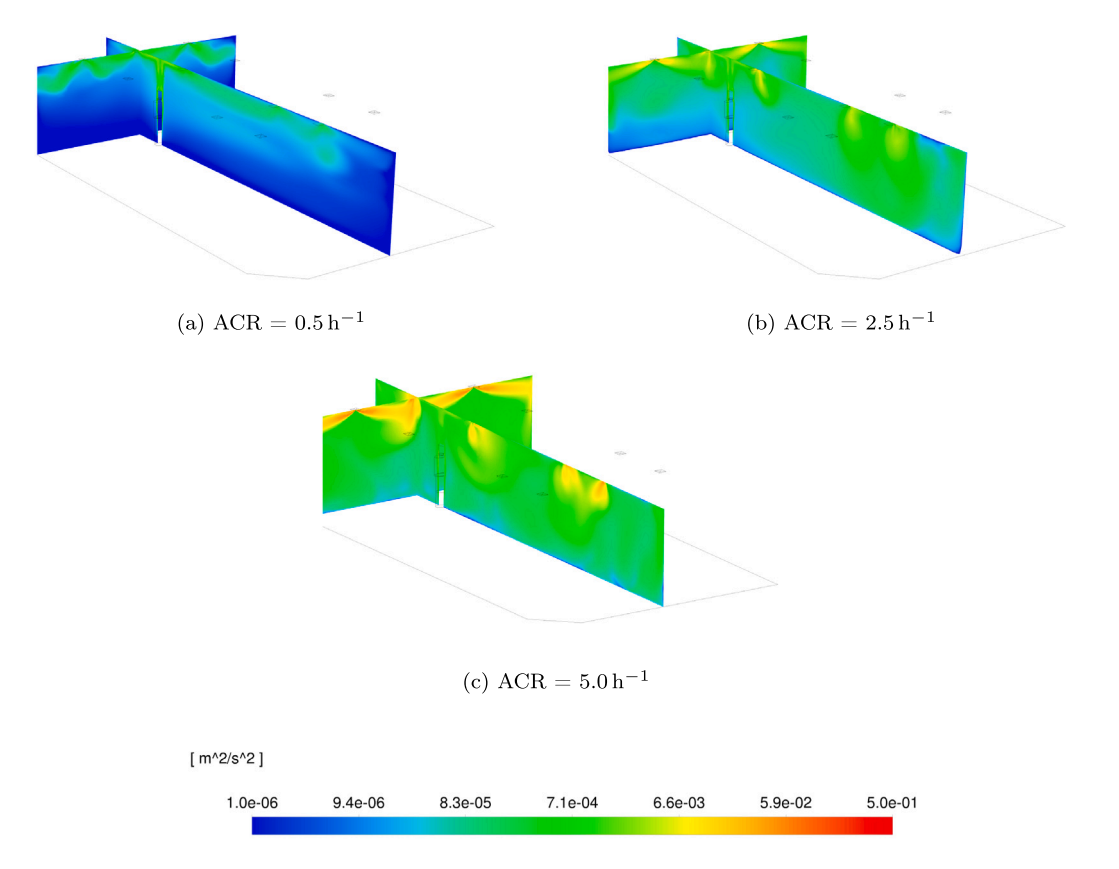


Fig. 6. Turbulent kinetic energy (on a log scale) on vertical planes through the middle of the person and one row of supply vents for all three ACRs. The upper limit was chosen to show the maximum turbulent kinetic energy in the $5\,h^{-1}$ model.

extracted via the ventilation system, with some remaining in the air after 30 min. Most of the intermediate size particles deposited on the floor, with only a small proportion being extracted via the ventilation system, even for the high ACR case shown.

It is suggested here that increasing the ACR, and consequently increasing the mixing or turbulence in the room, results in a reduction in the rate at which the intermediate size particles deposit. The same effect was report by Chao et al. [7]. Using CFD they showed that a higher ACR $(11.6\,h^{-1}\ vs\ 6.0\,h^{-1})$ resulted in less sedimentation of droplets in the $28\,\mu m$ to $45\,\mu m$ size range.

As discussed in the introduction, turbulence has been shown to increase deposition to surfaces [4,5,15] and to alter sedimentation rates [7] and settling velocities [21]. These effects depend on a number of factors including particle size. So, the global effect of increased ACR initially resulting in a slower reduction in viral concentrations in the room is reasonable. However, as stated above, the relative importance of this effect depends on how much virus is carried by the intermediate size particles (compared to that in the smallest sizes) and there is some uncertainty around this, as discussed previously.

3.4. Exposure

Exposure values are displayed in the following sections based on the time varying positions of the exhaled particles and the viral concentration in the particles. As discussed previously, there is a high level of uncertainty around both the exhaled droplet size distribution and the viral load distribution. As a result of this, the actual exposures in a real situation could be higher or lower than those shown here. There is also uncertainty around the dose–response for SARS-CoV-2. Therefore the reader should not interpret low exposure values as being safe or unimportant.

3.4.1. Exposure colour maps

The viral exposure was calculated across the domain within $(0.2 \text{ m})^3$ sub-volumes and this data is shown on a horizontal and vertical plane in Fig. 11, for exposures after 5 min and Fig. 12, for exposures after 30 min.

Increasing the ACR has a significant effect on the exposure across the room, with a higher ACR resulting in more mixing of the particles away from the person and into the room. This increase in mixing is apparent for both viral load definitions after 5 min. After 30 min when c_{SA} is used, the distribution of exposure still changes as the ACR increases, but the change is less dramatic.

The second interesting effect of increasing the ACR is how it affects the exposures around the exhaled jet. This can be seen in the vertical colour maps in Figs. 11 and 12. As the ACR increases and the ventilation flows reach into the lower part of the room, the exhaled jet is disrupted, so it penetrates a shorter distance towards the floor. This is the same effect that was described in relation to the particle tracks. The result of this would be less deposition of particles onto the floor, in the region of the exhaled jet, as the ACR increases.

Another feature, which can be seen in Figs. 11 and 12 is how the exposures are higher around the ceiling in the higher ACR cases, even though the thermal plume around the person is relatively stronger in the lower ACR cases, as shown in Fig. 5. This could be caused by one of two effects. Some disruption of the exhaled jet (by the airflow in the room) is required before a large number of the particles are mixed back towards the person and into their thermal plume. Or, the airflow in the bottom half of the room at the lowest ACR is not strong enough to carry the particles back to the person before they deposit onto the floor.

3.4.2. Exposure violin plots

Figs. 13 and 14 show violin plots with added box and whiskers, which illustrate the distribution of exposures, within the three 1 m

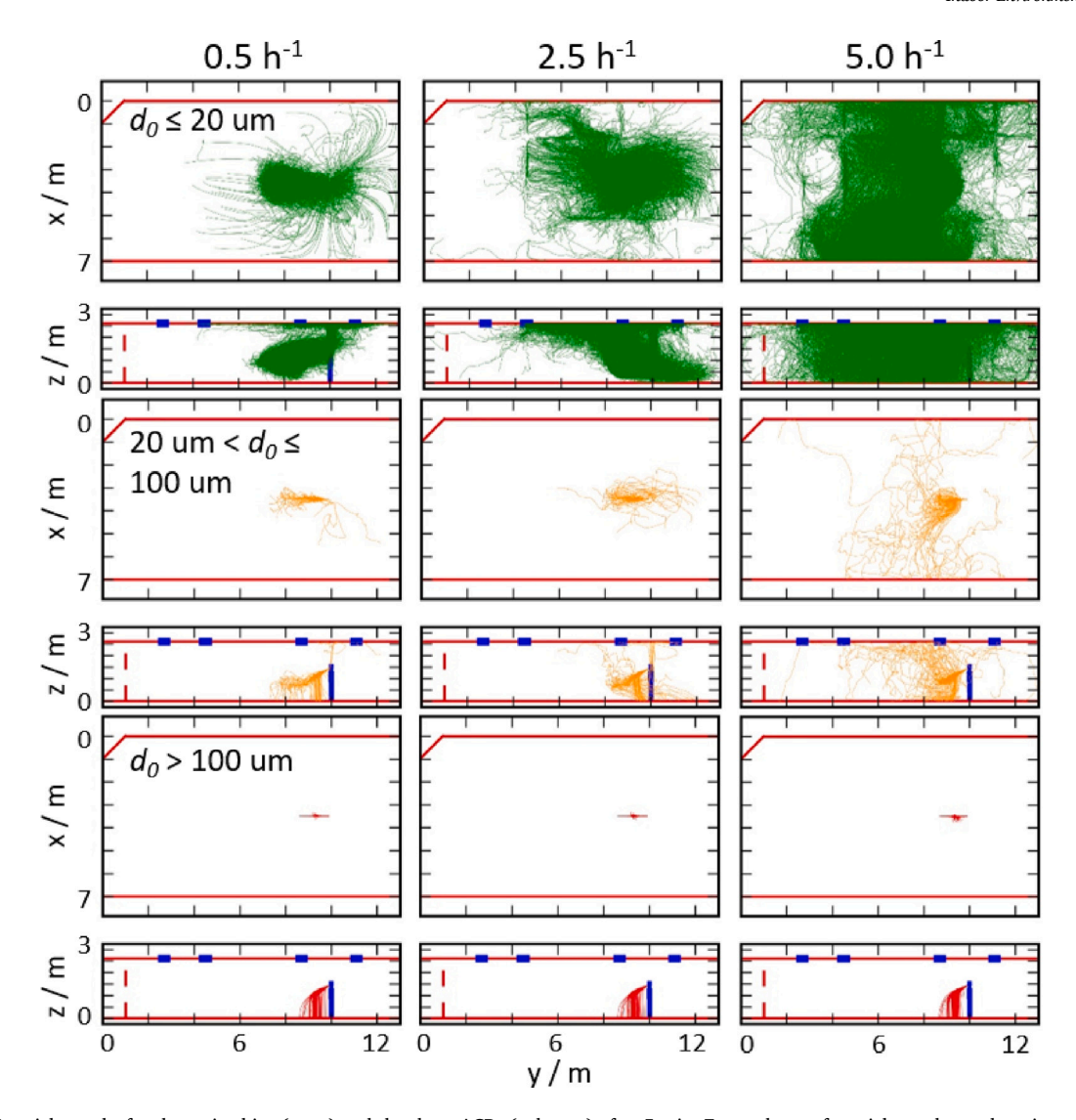


Fig. 7. Droplet/particle tracks for three size bins (rows) and the three ACRs (columns) after 5 min. For each set of particle tracks, a plan view and side-elevation are shown. The (bold) red solid or dashed lines indicate the walls of the room and the blue rectangles indicate the location of the extract vents. The particles tracks are for a single cough only.

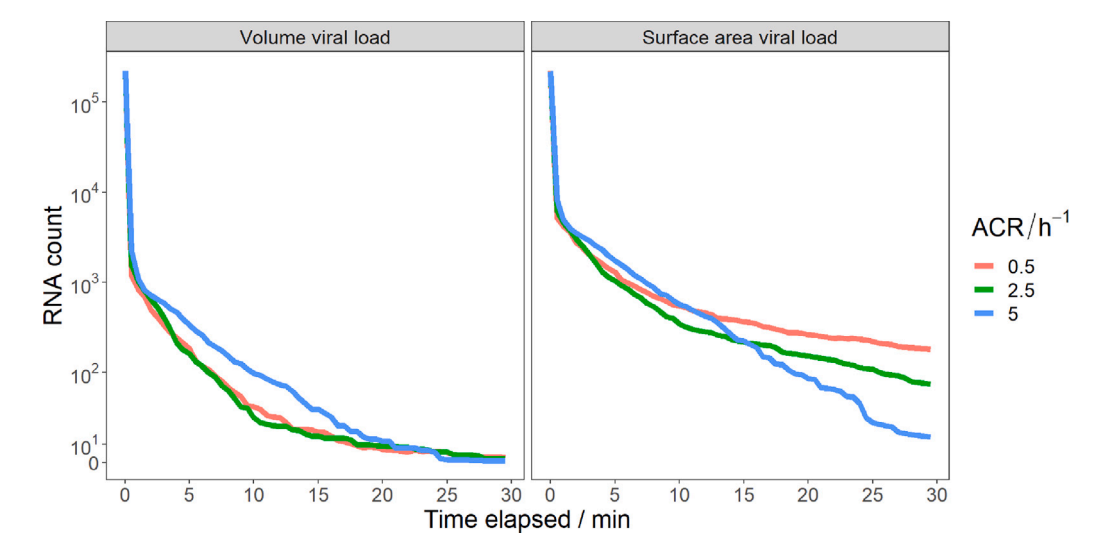


Fig. 8. Graphs showing how the total amount of viral RNA in the room changes with time for the three ACRs. Results are shown for the volume based viral load definition (left) and the droplet surface area definition (right). The total amount of virus exhaled in a single cough was 2.2×10^5 RNA copies. These graphs have a pseudo log scale which transitions from a log to a linear scale around zero.

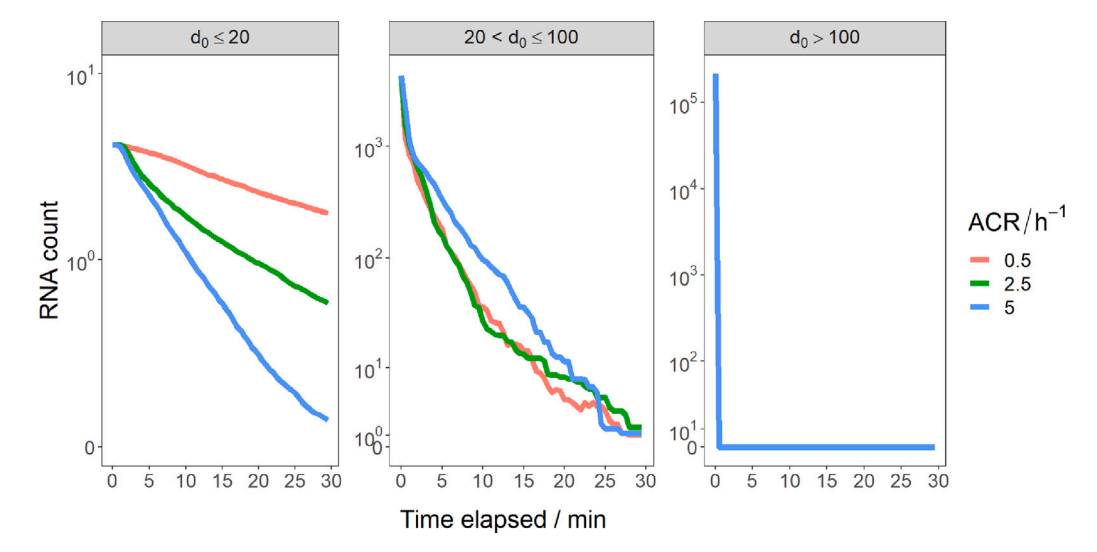


Fig. 9. Graphs showing how the total amount of viral RNA in the room changes with time for the three ACRs. Results are shown for the three size bins for the volume based viral load. These graphs have a pseudo log scale which transitions from a log to a linear scale around zero.

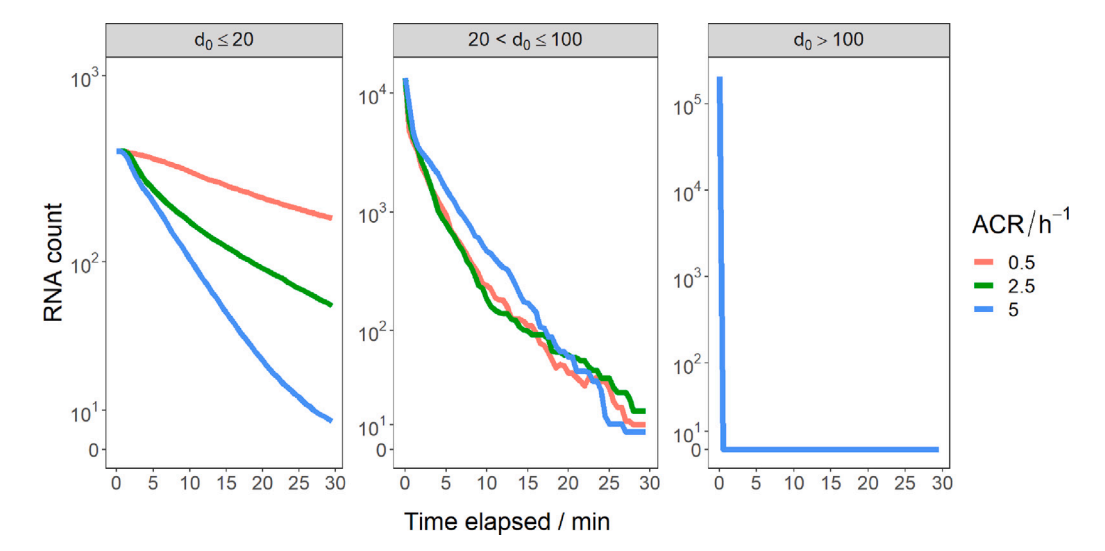


Fig. 10. Graphs showing how the total amount of viral RNA in the room changes with time for the three ACRs. Results are shown for the three size bins for the surface area based viral load. These graphs have a pseudo log scale which transitions from a log to a linear scale around zero.

x 1 m x 1 m analysis volumes. The analysis volumes were centred vertically and laterally on the mouth, so covered a height from 0.93 to 1.93 m. The positioning was chosen to represent the regions in which a susceptible person, who is standing directly in front of the infected person, may be breathing from. This represents a worst case in terms of the direction of the exhaled jet of droplets. For each 1 m³ analysis volume the exposure was calculated in 512 x (0.125 m)³ sub-volumes (i.e. approximately 2 litres, which could be considered to represent the region that a person breathes from). The box and whisker boxes extend from the first to the third quartile, so that the height of the box is the interquartile range. The upper/lower whisker extends up from the top/bottom of the box to the third quartile plus/minus 1.5 times the interquartile range, or the maximum/minimum data point (whichever is lower). Data outside of the upper whisker is shown as individual points. The violins provide additional information on how the data is distributed, i.e. it is rarely unimodal.

Using the same method as described in [20] a quantile regression model was used to determine whether there were statistically significant differences in the median log RNA exposures between the variables of interest.

The summary statistics from Figs. 13 and 14 are given in the supplementary material along with data for the effect of ACR on RNA exposure when results from all three $1\,\mathrm{m}^3$ boxes are combined. The data from all three boxes combined is also given in Table 1.

In all cases, after 5 min or 30 min and with either viral load definition, the median exposure is lower 2–3 m from the person compared to 0–1 m away. However, the exposure is not always lower 1–2 m from the person compared to 0–1 m away. The same varied effect with distance was shown in [20], where a range of different temperatures and relative humidities were studied, all with an ACR of $5\,h^{-1}$. These results highlights the importance of 2 m social distancing.

Even though the effect of distance from the person on the median exposure is varied, increased distance always reduces the upper whisker value (third quartile plus 1.5 times the interquartile range) and the exposure values above the upper whisker. Therefore, the likelihood of receiving a particularly high exposure is reduced as you move away from the person.

As with the exposure colour maps, Figs. 13 and 14 show a general trend of increased exposure as the ACR is increased (i.e. compare median, first or third quartile values, for each volume in turn, as the ACR is increased). This effect is not present when comparing all cases,

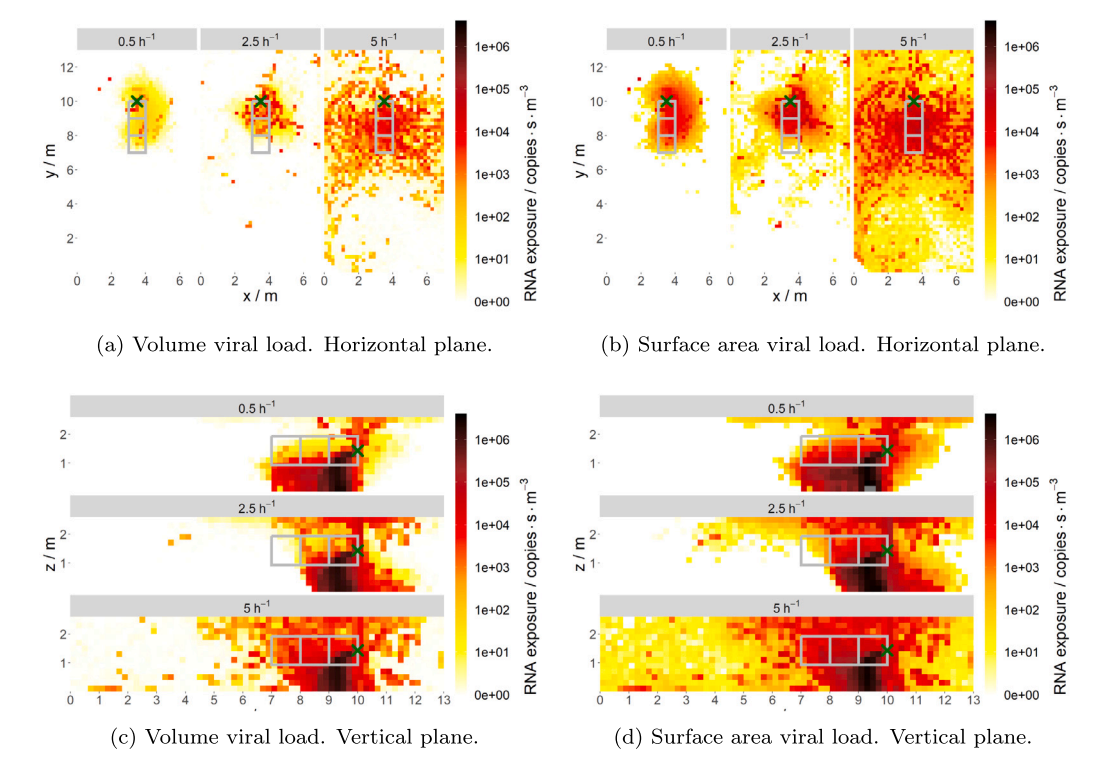


Fig. 11. Colour maps of viral RNA exposure after 5 min at the three ACRs, on a horizontal plane at z = 1.4 m and a vertical plane through the middle of the room. Results for volume based viral load are shown on the left and droplet surface area based viral load in the right. The 'X' indicates the location of the coughing person and the three grey boxes show the location of the 1 m³ volumes used in the following analysis. The colour bar has a pseudo log scale which transitions from a log to a linear scale around zero, with zero values shown as white.

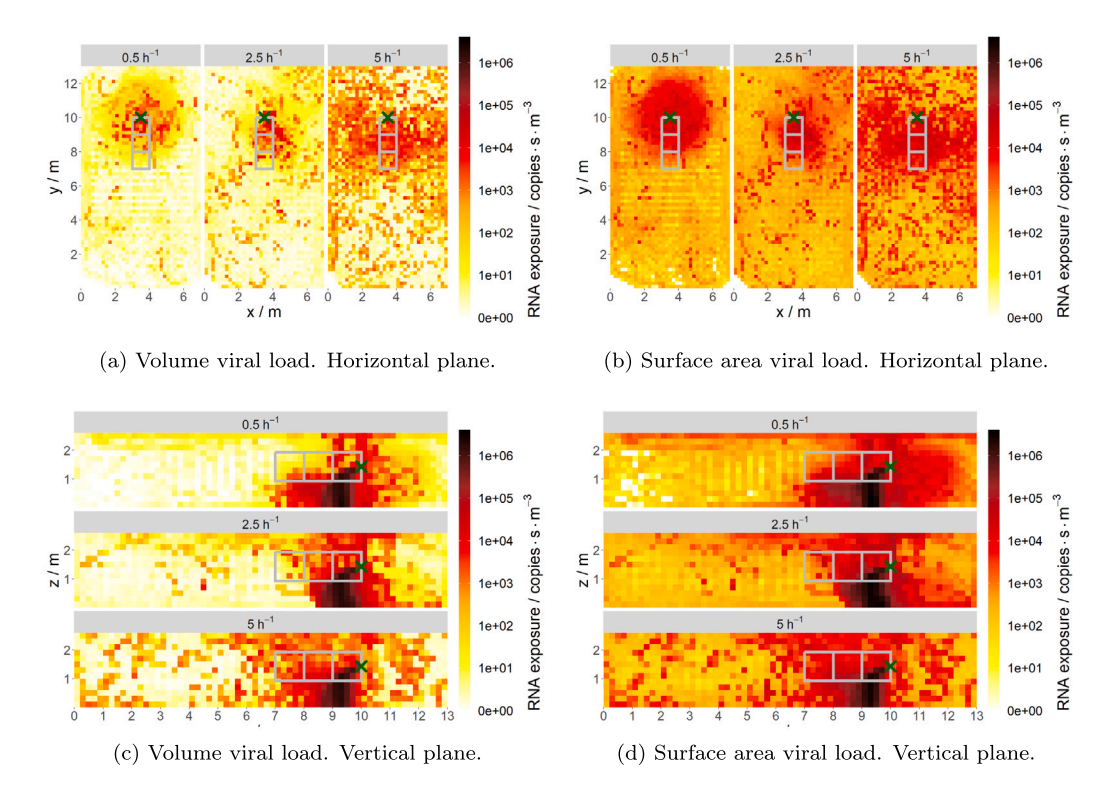
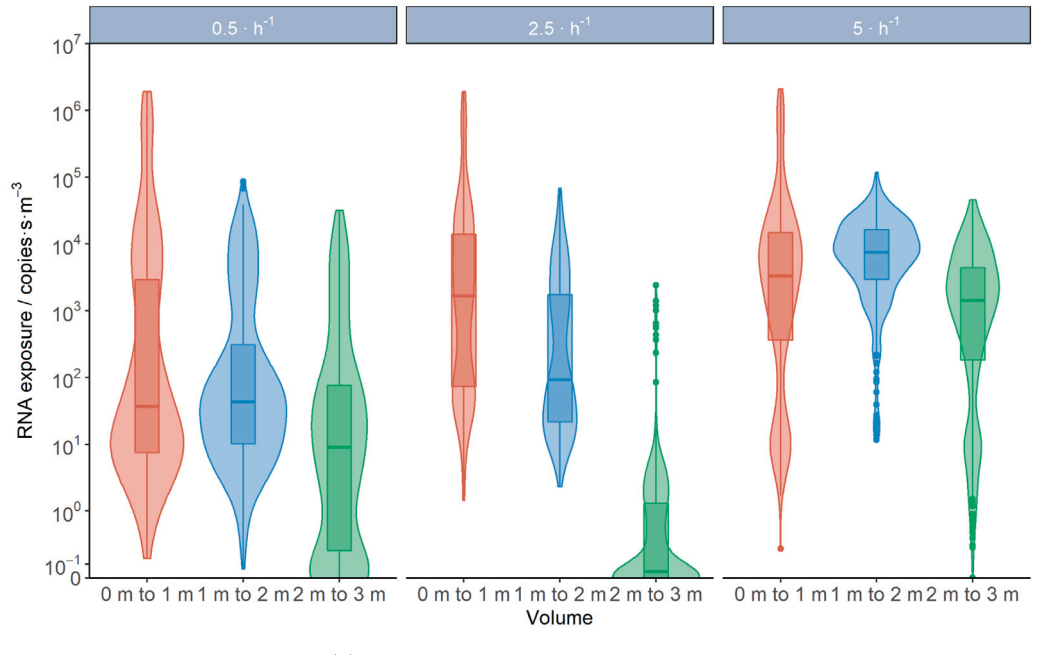
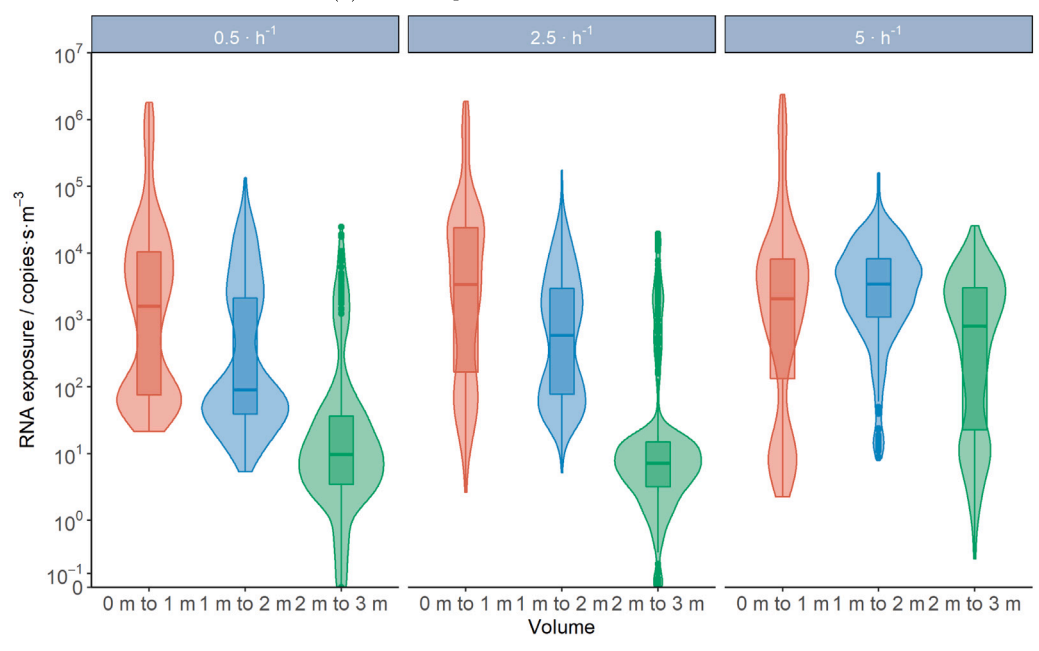


Fig. 12. Colour maps of viral RNA exposure after 30 min at the three ACRs. Further description is given in Fig. 11 caption.



(a) 5 min exposure. Volume viral load.



(b) 30 min exposure. Volume viral load.

Fig. 13. Violin plots (with added box and whiskers) for exposure showing the effect of distance from the infected person and the ACR. The susceptible person is assumed to be standing directly in front of the infected person. Data is for a droplet volume based viral load.

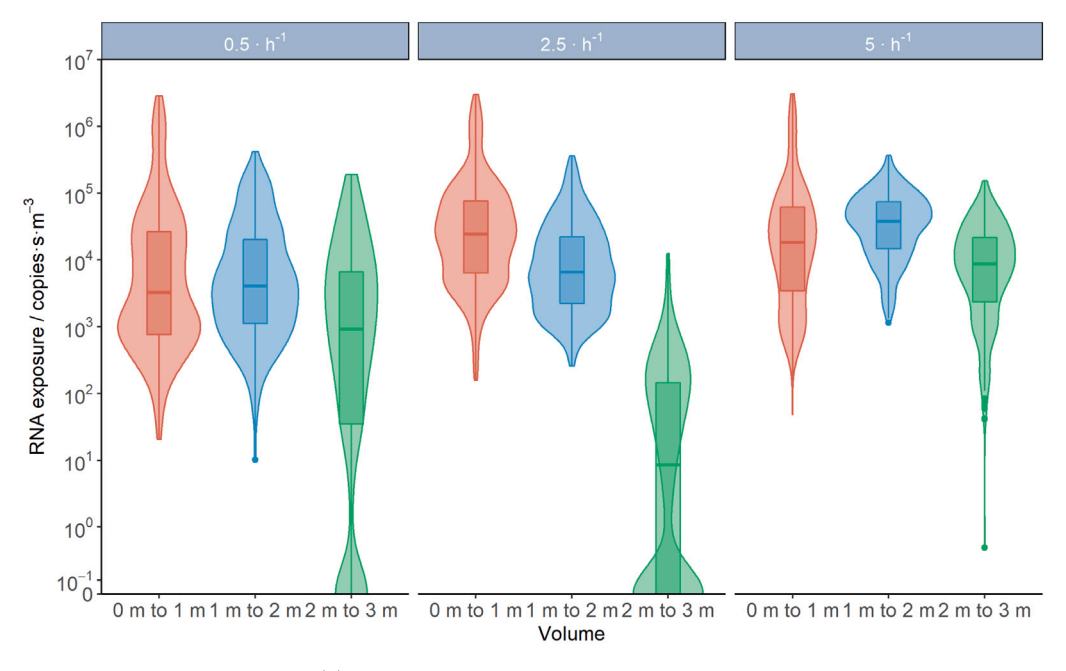
for example the median exposure is always lower in the 2–3 m volume when the ACR is $2.5\,h^{-1}$ vs $0.5\,h^{-1}$. This inconsistent trend is most likely due to the complex changes in the flow patterns in the room which occur as the ventilation rate increases. However, when the data from all three analysis volumes are combined together there is always a statistically significant increase (p <0.001 in all cases apart from one, where p = 0.004) in exposure with ACR.

As discussed in the introduction, an increase in exposure with an increase in ventilation rate has been shown before for an aircraft [8] and a mechanically ventilated room [10,16], although none of these studies presented data in the form of viral exposure, nor showed the distribution of possible exposures.

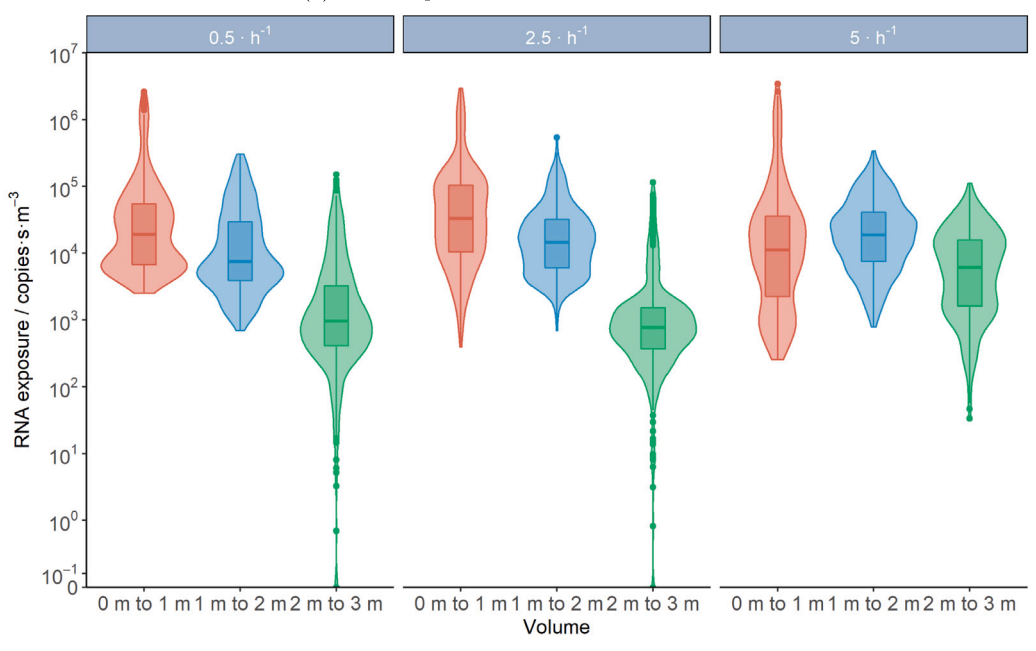
The increase in exposure with ACR is less when comparing 30 min data than it is with 5 min data. It is also less when comparing data for the surface area based viral load to that for a volume based viral load.

Table 1 show the median exposure across all three analysis volumes. The combined median exposure is 136 times larger at $5.0\,h^{-1}$ compared to $0.5\,h^{-1}$, for a volume based viral load after 5 min. For a viral load based on the surface area, the combined median exposure after 30 min was a factor of two higher at $5.0\,h^{-1}$ than it is at $0.5\,h^{-1}$.

The median, lower quartile and upper quartile exposures are always higher when c_{SA} is used compared to when c_V is used (excluding one lower quartile value when both viral load definitions give a zero value) and the values are often as much as two orders of magnitude higher.



(a) 5 min exposure. Surface area viral load.



(b) 30 min exposure. Surface area viral load.

Fig. 14. Violin plots (with added box and whiskers) for exposure showing the effect of distance from the infected person and the ACR. The susceptible person is assumed to be standing directly in front of the infected person. Data is for a surface area based viral load.

Table 1
Median exposure from all three analysis volumes combined after 5 min and 30 min and with volume based viral load and surface area base viral load.

	Median exposure / RNA copies s m ⁻³			
ACR	5 min		30 min	
/ h-1	c_V	c_{SA}	c_V	c_{SA}
0.5	26.4	2514.7	69.6	6365.1
2.5	42.5	4015.9	164.8	8970.5
5.0	3548.2	18240.2	1852.1	11 645.9

This is because the surface area based definition for the viral load results in more virus in the small particles and proportionally less in the biggest droplets, which deposit out very quickly. This is another reason why it is important to accurately define the viral load distribution as a function of the initial droplet diameter.

3.5. Discussion

In summary, there are at least three effects at play as the ACR is increased.

1. Increased mixing and transport leading to faster spread of droplets across the room.

- Increased turbulence and mixing resulting in reduced deposition of intermediate size particles.
- 3. Increased supply of fresh air, which dilutes the airborne virus.

The first of these will affect all airborne particles, but is only significant up to the time where dilution by fresh air becomes important. The second is most significant for intermediate size particles and so is strongly influenced by the exhaled droplet size distribution and the viral load. The third effect, which is the only one that is considered in most guidance on ventilation, is less important soon after the exhalation and/or close to the infected person, but is likely to dominate after long time periods when dilution effects will predominate.

The exhaled droplet size distribution and the viral load definition are key parameters. As mentioned previously, the amount of virus in the small aerosol particles could be proportionally higher still than that specified with the droplet surface area viral load definition, as suggested in [22,23].

As noted in the introduction, much guidance on infection control is based on the well-mixed assumption (where any contaminant is instantaneously mixed uniformly across a space). If this assumption is applied, the first two effects mentioned previously are no longer considered, so ventilation has only a positive effect. However, the results of this CFD modelling clearly show that this room has not become well-mixed within 30 min.

An important model simplification to raise here is that the movement of the infectious or susceptible people were not included. The effect of this movement would be to increase mixing local to the person so the significance of the mixing effect of the ventilation, both to transport material across the room and to reduce sedimentation, would be lessened.

The mixing effect of people movement can be large, for example Mingotti et al. [41] showed that the eddy diffusion coefficient (which describes the rate of mixing) as a result of people moving in a busy corridor could be from 0.01 to $0.1\,\mathrm{m}^2\,\mathrm{s}^{-1}$. This is one or two orders of magnitude higher than typical eddy diffusion coefficients in rooms without people movement [41]. Lim et al. [42] showed that people movement had a significant effect on room-scale air movement and tracer dispersion when the ceiling height was 3 m. However, when the ceiling height was 9 m, people movement only affected the local airflow. There could also be situations where there is not much people movement, for example in a work meeting, where staff are seated in an office or a classroom setting. Even static susceptible people would alter the flow locally. For example, their thermal plumes could help carry the virus carrying particles up towards the extract vents.

The addition of fans or local air conditioners in a room is also likely to increase the mixing as they would increase air velocities in the room. While we have not modelled this case, it is likely that use of a fan in a poorly ventilated room could result in greater dispersion of virus but without the mechanisms for dilution and removal that ventilation brings. Analysis of transmission in a coffee shop in Korea [43] and an outbreak in a restaurant in Guangzhou in China [44] both suggested that the high air velocities and directional flow due to air conditioners in poorly ventilated spaces enabled transmission over greater than expected distances.

If a room contained furniture, this could have an impact on both the airflow and the particle dispersion. The presence of furniture would tend to slow the airflow, therefore reducing the spread of the particles, and provide increased surface area for deposition. This could result in lower airborne exposures. However, contaminated surfaces could result in increased fomite transmission.

As the susceptible people were not included in the model, it does not account for the effect that their thermal plume may have on their exposure. A decision was made to simplify the model by not including the susceptible people, people movement or furniture to allow for more generic conclusions to be drawn. Not having the susceptible people explicitly represented in the model also allowed the exposure to be calculated at any location in the room. The effect of these simplifications could be explored in future work.

It is worth noting that the modelling carried out here is of a mechanically ventilated room with mixing ventilation delivered via the ceiling. The results may change if the mechanical ventilation design is different, for example if there is an extract vent close to the infectious person, or if the room has displacement ventilation. For comparison, the effect of some alternative ventilation strategies in a dental clinic is described by Yao et al. [19].

In a building with natural ventilation provided by open windows etc. (e.g. an older construction school or doctor's surgery) the effect of ACR on exposure may be different. If there is flow across the room from one window to another and if the infected person is sitting upwind of an uninfected person, then an increase in the ventilation rate would transfer the material more quickly and so potentially increase the exposure for the uninfected person. If the location of the people was switched, then increased ventilation would carry the virus away and out of the window more quickly, so the exposure for the uninfected person would be reduced.

This work could be extended in the future to consider the effects described above, as well as others such as: non-adiabatic walls and radiative heat transfer. A summary of the key model simplifications/limitations is given in Section 2.5.

The processed CFD data from this work could be used for other modelling studies, such as those using quantitative microbial risk assessment (QMRA) models. These types of model are used to explore the relative importance of different routes of transmission alongside options for mitigation methods. Including this data would allow the important short-term effect of ventilation on close-range exposure to be better represented. The data provides the spatial and temporal variation in exposure at the three ACRs and some data is also available with different ambient temperatures and relative humidities. Data from Figs. 13 and 14 is available in the supplementary material. Additional data is available on reasonable request.

4. Conclusions

A series of URANS CFD models were run to predict the effect of the air change rate on the airborne exposure to SARS-CoV-2 from a coughing person in a mechanically ventilated meeting with mixing ventilation. The conclusions from the work are given in the following subsections.

4.1. Particle dispersion

- Both small particles, $d_0 \le 20\,\mu\text{m}$, and intermediate size particles, $20\,\mu\text{m} < d_0 \le 100\,\mu\text{m}$, were shown to be mixed more effectively around the room as the ACR was increased from 0.5 to $5.0\,\text{h}^{-1}$.
- Particles with d₀ >100 μm did not appear to be affected by changes in the ACR.

4.2. Total viral count in the room

- Analysis of the total viral count in the room showed that the loss rate for the virus carried in the smallest particles (via both deposition onto surfaces and by extraction from the room via the ventilation system) increased as the ACR increased.
- For the intermediate size particles the effect was reversed, with the slowest loss rate seen with the highest ACR, up to approximately 15 or 20 min after the cough.
- The slower loss rate for the intermediate sizes was due to reduced deposition to the floor as a result of increased mixing in the room.

4.3. Exposure and ventilation rate

- For both viral concentration definitions (c_V and c_{SA}) an increase in the ACR resulted in generally higher exposures around the room.
- The combined exposure data from 0–3 m in front of the infected person showed a consistent and statistically significant increase as the ACR was increased.
- The effect of ventilation on exposure was less apparent when the viral load was based on c_{SA} and after 30 min.
- When the data was analysed separately in three 1 m³ volumes in front of the person, the effect of ACR on exposure was more varied
- The magnitude of the change in exposure reduces with time and this then brings it into line with most previous studies and guidance, which state that increasing ventilation reduces transmission risk. This suggests that the benefits of increased ventilation are likely to be most significant when an infected person is in a room for a long period of time and virus in the air could be considered to be well-mixed.

4.4. Exposure and distance from the infected person

- For all three ACRs, the median exposure was lower 2–3 m from the person, compared to 0–1 m from the person.
- However, the median exposure was not always lower 1–2 m from the person compared to 0–1 m away.
- The extreme (high) exposure values always decreased with distance from the person.
- These results highlight the importance of 2 m social distancing.

4.5. Exposure and viral load definition

• The median, lower quartile and upper quartile exposures are always higher when c_{SA} is used compared to when c_V is used (excluding one lower quartile value when both viral load definitions give a zero value) and the values are often as much as two orders of magnitude higher.

This is one of only a few CFD studies that have focussed on the close-range and short duration effects of ACR on particle transport. It is perhaps the only one to have estimated viral exposure using two different definitions for the viral load, and to have calculated the statistical significance of any correlations. While simplifying assumptions have been made in this study, perhaps most significantly the exclusion of the effect of people movement or the presence of the susceptible people, it does highlight the potentially detrimental effect that ventilation may have on airborne exposure over short periods of time. It is suggested that more work is carried out in this area, ideally a combination of experimental and modelling work, to explore the short duration effect of the ventilation rate on airborne transmission of disease.

CRediT authorship contribution statement

Timothy Foat: Writing – original draft, Visualization, Validation, Methodology, Conceptualization. Benjamin Higgins: Writing – review & editing, Visualization, Validation, Software, Investigation, Formal analysis. Suzie Abbs: Writing – review & editing, Visualization, Software, Methodology, Formal analysis. Thomas Maishman: Writing – review & editing, Visualization, Methodology, Formal analysis. Liam Gray: Writing – review & editing, Validation, Methodology. Adrian Kelsey: Writing – review & editing, Software, Methodology. Simon Coldrick: Software, Methodology. Alexander Edwards: Investigation, Formal analysis. Matthew J. Ivings: Writing – review & editing, Supervision, Conceptualization. Simon T. Parker: Writing – review & editing, Supervision, Methodology, Conceptualization. Catherine J. Noakes: Writing – review & editing, Supervision, Conceptualization.

Declaration of competing interest

The authors declare that they have no known competing financial interests or personal relationships that could have appeared to influence the work reported in this paper.

Acknowledgements

This paper and the research it describes were funded by the PRO-TECT COVID-19 National Core Study on transmission and environment, which was managed by HSE on behalf of HM Government. Its contents, including any opinions and/or conclusions expressed, are those of the authors alone and do not necessarily reflect Government or HSE policy. The authors would like to thank Dr Rory Hetherington (Health and Safety Executive) for his useful input into discussions on the modelling.

Content includes material subject to Crown Copyright © [2025]. Published by Elsevier Ireland Ltd. This is an open access article under the Open Government Licence (OGL) http://www.nationalarchives.gov.uk/doc/open-government-licence/version/3.

Appendix A. Supplementary data

Supplementary material related to this article can be found online at https://doi.org/10.1016/j.indenv.2025.100129.

References

- CIBSE, COVID-19: Ventilation, 2021, URL https://www.cibse.org/knowledge-research/knowledge-portal/covid-19-guidance-ventilation-v4.
- [2] UKHSA, Ventilation to reduce the spread of respiratory infections, including COVID-19, 2022, URL https://www.gov.uk/guidance/ventilation-to-reduce-thespread-of-respiratory-infections-including-covid-19.
- [3] E. Riley, G. Murphy, R. Riley, Airborne spread of measles in a suburban elementary school, Am. J. Epidemiol. 107 (5) (1978) 421–432, http://dx.doi. org/10.1093/oxfordjournals.aje.a112560.
- [4] A.C. Lai, W.W. Nazaroff, Modeling indoor particle deposition from turbulent flow onto smooth surfaces, J. Aerosol Sci. 31 (4) (2000) 463–476, http://dx.doi.org/ 10.1016/S0021-8502(99)00536-4.
- [5] T.L. Thatcher, A.C. Lai, R. Moreno-Jackson, R.G. Sextro, W.W. Nazaroff, Effects of room furnishings and air speed on particle deposition rates indoors, Atmos. Environ. 36 (11) (2002) 1811–1819, http://dx.doi.org/10.1016/\$1352-2310(02) 00157-7.
- [6] H. Furuya, Risk of transmission of airborne infection during train commute based on mathematical model, Environ. Heal. Prev. Med. 12 (2) (2007) 78–83, http://dx.doi.org/10.1265/ehpm.12.78.
- [7] C. Chao, M. Wan, G. Sze To, Transport and removal of expiratory droplets in hospital ward environment, Aerosol Sci. Technol. 42 (5) (2008) 377–394, http://dx.doi.org/10.1080/02786820802104973.
- [8] G.N. Sze To, M.P. Wan, C.Y.H. Chao, L. Fang, A. Melikov, Experimental study of dispersion and deposition of expiratory aerosols in aircraft cabins and impact on infectious disease transmission, Aerosol Sci. Technol. 43 (5) (2009) 466–485.
- [9] G.N. Sze To, C.Y.H. Chao, Review and comparison between the Wells-Riley and dose-response approaches to risk assessment of infectious respiratory diseases, Indoor Air 20 (1) (2010) 2–16, http://dx.doi.org/10.1111/j.1600-0668.2009. 00621.x.
- [10] J. Pantelic, K.W. Tham, Adequacy of air change rate as the sole indicator of an air distribution system's effectiveness to mitigate airborne infectious disease transmission caused by a cough release in the room with overhead mixing ventilation: a case study, HVACR Res. 19 (8) (2013) 947–961.
- [11] H. Dai, B. Zhao, Association of the infection probability of COVID-19 with ventilation rates in confined spaces, in: Building Simulation, vol. 13, no. 6, Springer, 2020, pp. 1321–1327, http://dx.doi.org/10.1007/s12273-020-0703-5.
- [12] Y. Liu, Z. Ning, Y. Chen, M. Guo, Y. Liu, N.K. Gali, L. Sun, Y. Duan, J. Cai, D. Westerdahl, et al., Aerodynamic analysis of SARS-CoV-2 in two Wuhan hospitals, Nature 582 (7813) (2020) 557–560.
- [13] J. Jimenez, Z. Peng, COVID-19 aerosol transmission estimator, 2021, URL https: //tinyurl.com/covid-estimator.
- [14] L. Rocha-Melogno, K. Crank, K. Bibby, G. Gray, M. Deshusses, Aerosol-mediated infectious disease risk assessments, 2021, URL https://rapidqmra.shinyapps.io/ Rapid OMRA/.
- [15] B. Blocken, T. van Druenen, A. Ricci, L. Kang, T. van Hooff, P. Qin, L. Xia, C.A. Ruiz, J. Arts, J. Diepens, et al., Ventilation and air cleaning to limit aerosol particle concentrations in a gym during the COVID-19 pandemic, Build. Environ. 193 (2021) 107659, http://dx.doi.org/10.1016/j.buildenv.2021.107659.

- [16] J. Wei, L. Wang, T. Jin, Y. Li, N. Zhang, Effects of occupant behavior and ventilation on exposure to respiratory droplets in the indoor environment, Build. Environ. (2023) 109973.
- [17] J. Li, S. Zuraimi, S. Schiavon, Should we use ceiling fans indoors to reduce the
- [18] B. Omerzo, T. Zakula, L.R. Glicksman, Experimental and CFD study of air distribution system and airflow rate impact on airborne transmission across different occupancy patterns, Build. Environ. (2025) 112588.
- [19] G. Yao, H. Xu, H. Liu, Z. Liu, C. Jiang, W. Zhuang, Y. Li, J. Liu, J. He, Effectiveness of different ventilation strategies for mitigating airborne pathogen transmission in a multi-compartment dental clinic, J. Build. Eng. 106 (2025) 112602
- [20] T. Foat, B. Higgins, S. Abbs, T. Maishman, S. Coldrick, A. Kelsey, M. Ivings, S. Parker, C. Noakes, Modelling the effect of temperature and relative humidity on exposure to SARS-CoV-2 in a mechanically ventilated room, Indoor Air 32 (11) (2022) e13146
- [21] G. Good, P. Ireland, G. Bewley, E. Bodenschatz, L. Collins, Z. Warhaft, Settling regimes of inertial particles in isotropic turbulence, J. Fluid Mech. 759 (2014) http://dx.doi.org/10.1017/jfm.2014.602.
- [22] D.K. Milton, M.P. Fabian, B.J. Cowling, M.L. Grantham, J.J. McDevitt, Influenza virus aerosols in human exhaled breath: particle size, culturability, and effect of surgical masks, PLoS Pathog. 9 (3) (2013) e1003205.
- [23] K.K. Coleman, D.J.W. Tay, K.S. Tan, S.W.X. Ong, T.S. Than, M.H. Koh, Y.Q. Chin, H. Nasir, T.M. Mak, J.J.H. Chu, et al., Viral load of severe acute respiratory syndrome coronavirus 2 (SARS-CoV-2) in respiratory aerosols emitted by patients with coronavirus disease 2019 (COVID-19) while breathing, talking, and singing, Clin. Infect. Dis. 74 (10) (2022) 1722–1728.
- [24] S. Coldrick, A. Kelsey, M.J. Ivings, T.G. Foat, S.T. Parker, C.J. Noakes, A. Bennett, H. Rickard, G. Moore, Modeling and experimental study of dispersion and deposition of respiratory emissions with implications for disease transmission, Indoor Air 32 (2) (2022) e13000, http://dx.doi.org/10.1111/ina.13000.
- [25] D.M. Murray, D.E. Burmaster, Residential air exchange rates in the United States: empirical and estimated parametric distributions by season and climatic region, Risk Anal. 15 (4) (1995) 459–465, http://dx.doi.org/10.1111/j.1539-6924.1995.tb00338.x.
- [26] M. Deevy, N. Gobeau, CFD modelling of benchmark test cases for a flow around a computer simulated person, 2006, https://webarchive.nationalarchives.gov. uk/ukgwa/20230103131424/https://www.hse.gov.uk/research/hsl/ochealth.htm. Health and Safety Executive, HSL/2006/51.
- [27] S. Coldrick, A. Kelsey, L. Gray, R. Hetherington, M. Ivings, Understanding SARS-CoV-2 transmission: Computational fluid dynamics modelling of respiratory particles, 2023, https://sites.manchester.ac.uk/covid19-nationalproject/2023/07/21/understanding-sars-cov-2-transmission-computational-fluiddynamics-modelling-of-respiratory-particles/. Health and Safety Executive.
- [28] P. Nielsen, S. Murakami, S. Kato, C. Topp, J. Yang, Benchmark Tests for a Computer Simulated Person, Technical Report, Aalborg University, Indoor Environmental Engineering, 2003.
- [29] H.J. Hussein, S.P. Capp, W.K. George, Velocity measurements in a high-Reynoldsnumber, momentum-conserving, axisymmetric, turbulent jet, J. Fluid Mech. 258 (1994) 31–75.

- [30] J. Srebric, Q. Chen, Simplified numerical models for complex air supply diffusers, HVACR Res. 8 (3) (2002) 277–294.
- [31] S. Zhu, S. Kato, J.-H. Yang, Study on transport characteristics of saliva droplets produced by coughing in a calm indoor environment, Build. Environ. 41 (12) (2006) 1691–1702.
- [32] G. Johnson, L. Morawska, Z. Ristovski, M. Hargreaves, K. Mengersen, C.H. Chao, M. Wan, Y. Li, X. Xie, D. Katoshevski, et al., Modality of human expired aerosol size distributions, J. Aerosol Sci. 42 (12) (2011) 839–851, http://dx.doi.org/10.1016/j.jaerosci.2011.07.009.
- [33] M.E. Stettler, R.T. Nishida, P.M. de Oliveira, L.C. Mesquita, T.J. Johnson, E.R. Galea, A. Grandison, J. Ewer, D. Carruthers, D. Sykes, et al., Source terms for benchmarking models of SARS-CoV-2 transmission via aerosols and droplets, R. Soc. Open Sci. 9 (5) (2022) 212022.
- [34] S. Parker, T. Foat, S. Preston, Towards quantitative prediction of aerosol deposition from turbulent flows, J. Aerosol Sci. 39 (2) (2008) 99–112.
- [35] J.K. Gupta, C.-H. Lin, Q. Chen, Flow dynamics and characterization of a cough, Indoor Air 19 (6) (2009) 517–525.
- [36] J. Duguid, The size and the duration of air-carriage of respiratory droplets and droplet-nuclei, Epidemiol. Infect. 44 (6) (1946) 471–479.
- [37] S.R. Hanna, O.R. Hansen, S. Dharmavaram, FLACS CFD air quality model performance evaluation with Kit Fox, MUST, prairie grass, and EMU observations, Atmos. Environ. 38 (28) (2004) 4675–4687.
- [38] X. Wang, G.B. Deane, K.A. Moore, O.S. Ryder, M.D. Stokes, C.M. Beall, D.B. Collins, M.V. Santander, S.M. Burrows, C.M. Sultana, et al., The role of jet and film drops in controlling the mixing state of submicron sea spray aerosol particles, Proc. Natl. Acad. Sci. 114 (27) (2017) 6978–6983.
- [39] A. Singanayagam, S. Hakki, J. Dunning, K.J. Madon, M.A. Crone, A. Koycheva, N. Derqui-Fernandez, J.L. Barnett, M.G. Whitfield, R. Varro, et al., Community transmission and viral load kinetics of the SARS-CoV-2 delta (B. 1.617. 2) variant in vaccinated and unvaccinated individuals in the UK: a prospective, longitudinal, cohort study, Lancet Infect. Dis. 22 (2) (2022) 183–195, http://dx.doi.org/10.1016/S1473-3099(21)00648-4.
- [40] S.J. Smither, L.S. Eastaugh, J.S. Findlay, M.S. Lever, Experimental aerosol survival of SARS-CoV-2 in artificial saliva and tissue culture media at medium and high humidity, Emerg. Microb. Infect. 9 (1) (2020) 1415–1417.
- [41] N. Mingotti, R. Wood, C. Noakes, A.W. Woods, The mixing of airborne contaminants by the repeated passage of people along a corridor, J. Fluid Mech. 903 (2020) A52.
- [42] H. Lim, T.G. Foat, S.T. Parker, C. Vanderwel, On the effects of walking speed, crowd density and human-to-source distance on pollutant dispersion in indoor spaces, Build. Environ. 259 (2024) 111649.
- [43] K.-S. Kwon, J.-I. Park, Y.J. Park, D.-M. Jung, K.-W. Ryu, J.-H. Lee, Evidence of long-distance droplet transmission of SARS-CoV-2 by direct air flow in a restaurant in Korea, J. Korean Med. Sci. 35 (46) (2020).
- [44] Y. Li, H. Qian, J. Hang, X. Chen, P. Cheng, H. Ling, S. Wang, P. Liang, J. Li, S. Xiao, et al., Probable airborne transmission of SARS-CoV-2 in a poorly ventilated restaurant. Build. Environ. 196 (2021) 107788.